Scaling structure and thermodynamics of strange sets

Mogens H. Jensen,* Leo P. Kadanoff, and Itamar Procaccia†
The James Franck Institute, The University of Chicago, Chicago, Illinois 60637
(Received 17 November 1986)

We present a quantitative theory of the scaling properties of Julia sets, using them as a case model for nontrivial fractal sets off the borderline of chaos. It is shown that generally the theory has a "macroscopic" part which consists of the generalized dimensions of the set, or its spectrum of scaling indexes, and a "microscopic" part which consists of scaling functions. These two facets are formally and computationally equivalent to thermodynamics and statistical mechanics in the theory of many-body systems. We construct scaling functions for the Julia sets and argue that basically there are two different approaches to this construction, which we term the Feigenbaum approach and the Ruelle-Bowen-Sinai approach. For the cases considered here the two approaches converge, meaning that we can map the theory onto Ising models with finite-range interactions. The largest eigenvalue of the appropriate transfer matrix furnishes the thermodynamic functions.

I. INTRODUCTION

The aim of a quantitative theory of nontrivial (i.e., non-self-similar) fractal sets is to provide tools for the predictions of the properties of the set based on some limited amount of information. For strictly self-similar sets this task is trivial; knowledge of a few steps of refinement of the set is sufficient for carrying on the refinement *ad infinitum*. Unfortunately (or fortunately?) fractal sets that appear in nature are often nontrivial and have a spectrum of scaling indexes. Sets of this kind are called multifractals.[1–8] These sets can be described in two fundamentally different ways. On the one hand, one can seek global descriptions which enable one to predict the overall properties of the multifractals. On the other hand, one should seek a more detailed type of approach which enables one to get a more detailed description of the local properties of the fractal. This distinction is similar to the distinction between thermodynamics and statistical mechanics. Thermodynamics provides characterization of macroscopic systems in terms of their intensive variables (temperature, pressure, etc.) and their thermodynamic functions (free energy, entropy, etc.). Statistical mechanics provides tools for the calculation of these functions from the knowledge of the Hamiltonian.

There have been several apparently independent threads of recent work in which statistical mechanics and thermodynamics have been employed to describe fractal behavior. Most explicitly, Ruelle,[9] Bowen,[10] and Sinai[11] have developed a highly mathematical formalism, most particularly for the fractals called Julia sets[12–14] (see below), in which one-dimensional statistical mechanics and thermodynamics play an essential role. Part of our work will follow from this approach (see also Refs. 15 and 16). An alternative approach is based on Feigenbaum's scaling functions, σ,[17] which furnishes an alternative source of a thermodynamic formalism.[18,19] We shall make the connection between these two approaches in this paper.

Recently, a phenomenological approach to the characterization of fractal sets which plays the role of thermodynamics has been proposed and advanced.[3,6–8] The basic idea is to consider a continuous spectrum of generalized dimensions. These are defined as follows:[3,7] Given a partition of the set into "balls" of radius l_i, one focuses on a measurable quantity p and measures its value in the ith ball, yielding a number p_i. For concreteness we shall focus here on one such measurable property, i.e., the probability measure. Next one forms the partition function

$$\Gamma(q,\tau)=\sum_i p_i^q/l_i^\tau \ . \tag{1.1}$$

Choosing a value of q, and seeking the supreme (infimum) of $\Gamma(q,\tau)$ for $q>1$ ($q<1$) over all partitions, one finds in the limit $\max l_i\to 0$ that $\Gamma(q,\tau)$ goes to infinity for $\tau>\tau(q)$ and to zero for $\tau<\tau(q)$. This defines the quantity

$$\tau(q)=(q-1)D_q \ , \tag{1.2}$$

where D_q is the generalized dimension.[3] In particular, $D_{q=0}$ is the Hausdorff dimension. It will be argued below that $\tau(q)$ [or rather $q(\tau)$] assumes for the problems at hand the role that the free energy has in thermodynamics.[18,19] The place of entropy and energy is taken by variables conjugate to τ and q, denoted in Refs. 7 and 8 by f and α. To see the meaning of these, consider a partition into a uniform grid of boxes of size l, and define α_i (Refs. 6 and 7) by

$$p_i=l^{\alpha_i} \ . \tag{1.3}$$

With the help of the pseudoprobability $g_i(q)$,

$$g_i(q)=l^{q\alpha_i}\Big/\sum_i l^{q\alpha_i} \ , \tag{1.4}$$

it is easy to see[20] that

$$\partial[\tau(q)]/\partial q=\sum_i g_i(q)\alpha_i=\langle\alpha\rangle(q) \ . \tag{1.5}$$

In addition, if $f(q)$ is defined by

$$f(\langle\alpha\rangle(q))=\sum g_i(q)\log g_i(q)/\log l \ , \tag{1.6}$$

then one has

$$f = q\partial[\tau(q)]/\partial q - \tau(q) \ . \tag{1.7}$$

Equations (1.4)–(1.7) are the "canonical" counterparts of the microcanonical definitions of Ref. 7. The analogy to statistical mechanics is obvious.

A question that was clarified only recently[18,19] is "what is the analog of the Hamiltonian, what is the microscopic information?" An answer is obtained by considering partitions such that $p_i = \text{const}$. If we have N_n boxes in the nth step of refinement of the set, then $p_i = N_n^{-1}$. Defining $\tau(q)$ by that value of τ for which $\Gamma(q,\tau)=1$, we get from (1.1) a relation

$$N_n^{q(\tau)} = \sum_i (l_i)^{-\tau} \ . \tag{1.8}$$

In general N_n grows exponentially, and we can write $N_n = a^n$. This means that we can arrange the N_n balls on a tree (binary for $a<2$, ternary for $2<a<3$, etc.), and write the index i as a sequence of binary, ternary, etc., numbers $(\varepsilon_1, \ldots, \varepsilon_n)$. Equation (1.8) then reads

$$a^{nq(\tau)} = \sum_{\varepsilon_n, \ldots, \varepsilon_1} [l(\varepsilon_n, \ldots, \varepsilon_1)]^{-\tau} \ . \tag{1.9a}$$

Performing two steps of refinement we get[11]

$$\sum_{\varepsilon_{n+1}, \ldots, \varepsilon_1} |\, l(\varepsilon_{n+1}, \ldots, \varepsilon_1)\,|^{-\tau} = a^{q(\tau)} \sum_{\varepsilon_n, \ldots, \varepsilon_1} |\, l(\varepsilon_n, \ldots, \varepsilon_1)\,|^{-\tau} \ . \tag{1.9b}$$

The microscopic information is carried now by the so-called scaling function,[17,19] $\sigma(\varepsilon_{n+1}, \ldots, \varepsilon_1)$, which is the daughter-to-mother ratio

$$l(\varepsilon_{n+1}, \ldots, \varepsilon_1)/l(\varepsilon_n, \ldots, \varepsilon_1) = \sigma(\varepsilon_{n+1}, \ldots, \varepsilon_1) \ . \tag{1.10}$$

Since the sets are in general non-self-similar, the scaling function σ depends in principle on the entire history $(\varepsilon_1, \ldots, \varepsilon_{n+1})$. For such cases we are not in a position to produce useful theories. If we find, however, a way that generates a scaling function that depends most strongly on the head (or the tail) of the symbol sequence, and very weakly on the tail (or head) of the sequence, we can proceed. By making the appropriate choice of the quantities $l(\varepsilon_n, \ldots, \varepsilon_1)$ one can produce a scaling function which depends most strongly upon the high-order digits of the symbol sequence. Hence in this case we can write the large-n scaling function as

$$\sigma(\varepsilon_n, \varepsilon_{n-1}, \ldots, \varepsilon_1) = \bar{\sigma}(\varepsilon_n, \varepsilon_{n-1}, \ldots) \ . \tag{1.10a}$$

However, we shall also consider a formalism in which the l's are chosen to make the function σ depend most strongly upon the first elements in the symbol sequence, and very weakly upon the last. In this case we write, instead of (1.10a),

$$\sigma(\varepsilon_n, \varepsilon_{n-1}, \ldots, \varepsilon_1) = \tilde{\sigma}(\varepsilon_1, \varepsilon_2, \varepsilon_3, \ldots) \tag{1.10b}$$

for large n. For now, we do not have to specify which case we are considering. Inserting (1.10) in (1.9) we get

$$\sum_{\varepsilon_{n+1}, \ldots, \varepsilon_1} \sigma(\varepsilon_{n+1}, \ldots, \varepsilon_1)\, |\, l(\varepsilon_n, \ldots, \varepsilon_1)\,|^{-\tau} = a^{q_n(\tau)} \sum_{\varepsilon_n, \ldots, \varepsilon_1} |\, l(\varepsilon_n, \ldots, \varepsilon_1)\,|^{-\tau} \ . \tag{1.11}$$

We find[18,19] that whenever the scaling function for large n depends only on one end of its symbol sequence, then as $n \to \infty$, $q_n(\tau) \to q(\tau)$. To see how this works note that Eq. (1.11) can be brought to an eigenvalue equation by adding summations and Kronecker δ functions:

$$\sum_{\substack{\varepsilon_{n+1}, \ldots, \varepsilon_1 \\ \varepsilon_n', \ldots, \varepsilon_2'}} \delta_{\varepsilon_n \varepsilon_n'} \cdots \delta_{\varepsilon_2 \varepsilon_2'} \sigma(\varepsilon_{n+1}, \ldots, \varepsilon_1)\, |\, l(\varepsilon_n', \ldots, \varepsilon_2', \varepsilon_1)\,|^{-\tau} = a^{q_n(\tau)} \sum_{\varepsilon_n, \ldots, \varepsilon_1} |\, l(\varepsilon_n, \ldots, \varepsilon_1)\,|^{-\tau} \ . \tag{1.12}$$

Define now the transfer matrix T by

$$\langle \varepsilon_{n+1}, \ldots, \varepsilon_2 \,|\, T \,|\, \varepsilon_n', \ldots, \varepsilon_2', \varepsilon_1 \rangle = \sigma(\varepsilon_{n+1}, \ldots, \varepsilon_1) \delta_{\varepsilon_n \varepsilon_n'} \cdots \delta_{\varepsilon_2 \varepsilon_2'} \ . \tag{1.13}$$

For large n, Eq. (1.12) can be considered an eigenvalue equation. If σ depends weakly upon either end of its symbol sequence, one can truncate the transfer matrix by simply neglecting the matrix indexes that do not appear in σ. In the large-n limit $a^{q_n(\tau)}$ becomes the largest eigenvalue of this truncated matrix.

$$a^{q(\tau)} = \lambda(\tau) \ . \tag{1.14}$$

In particular $\lambda(\tau)$ is independent of n. But this kind of formalism involving a transfer matrix and eigenvalues is the usual way of expressing problems in one-dimensional statistical mechanics. The mapping onto statistical mechanics is then complete. We have mapped the process of refinement of the set onto an Ising (or Potts) model problem where the length of memory in σ is the range of interaction and the number of values that ε_n takes on is the number of spin states. The thermodynamic information $q(\tau)$ is then calculable from the largest eigenvalue of the transfer matrix.

The mathematical aspects of the thermodynamic formalism were worked out in the papers of Ruelle,[9] Bowen,[10] and Sinai[11] (RBS). The most extensive calculations have been done for the strange sets that appear in dynamical systems at the borderline of chaos.[18,19] There are a few features that make these sets particularly easy: (i) They are embedded in one dimension, (ii) the Lyapunov number is 1, so that length scales are neither stretched nor contracted on the average, and (iii) they are well ordered in the sense that the orbits come close to a critical point of the mapping (where lengths contract

sharply) ever so rarely (in period doubling every 2^n iterations, for golden-mean orbits every Fibonacci number of iterations, etc.). The scaling functions could therefore be arranged to have exponential decay in their dependence on the symbol sequence.

In this paper we apply the scaling theory to strange sets that do not belong to the borderline of chaos. We choose to remain within dynamical systems because the theory of those is so much advanced compared to other fields in which strange, nontrivial sets appear. The examples that we decided to focus on are the Julia sets of analytic (conformal) mappings of the plane onto itself.[12-14] The Julia set is a strange repeller.[19] In the case considered here it is an invariant set which divides the plane into two parts: points that iterate to infinity and points that iterate to a stable fixed point. It is also an example of a "basin boundary."[20] The dynamics on the invariant set is chaotic in the sense that the orbits of two nearby points diverge exponentially. The advantage of this set compared to generic strange attractors is that we have adequate understanding of its symbolic dynamics, distribution of periodic orbits, etc. We thus relax some of the conditions that characterize systems at the borderline of chaos. The Lyapunov number is not 1, and the sets are embedded in two dimensions. However, they are quasi-one-dimensional because the mapping is conformal, and they are well ordered. It will be seen below how this facilitates the construction of a theory. The sets and their symbolic representations will be detailed in Sec. II.

In light of the Introduction above, it is clear that the first aim of the theory is to achieve scaling functions whose dependence on the symbol sequences converges fast (if possible, exponentially). We shall see that there is no unique way of obtaining such convergence. Basically there are, however, two fundamentally different approaches. One yields scaling functions that depend most strongly on the tail of the symbolic sequence. We call this the Feigenbaum approach, since this is the property of the Feigenbaum scaling functions for the period-doubling problem, for example.[12] The other approach results in scaling functions that depend most strongly on the head of the symbol sequence. We call this the RBS approach since it is intimately related to the thermodynamic theory of dynamical systems.[13-15] Although the two approaches converge in the case studied here, and in fact can be shown to be asymptotically equivalent, they are not going to be equivalent in general. The two approaches, their results, and their comparison are explained in Secs. III and IV.

The calculation of the thermodynamic quantities [i.e., $q(\tau)$] from the statistical mechanical counterpart is summarized in Sec. V. Section VI offers conclusions and comments on the road ahead.

II. THE JULIA SET

A. General remarks

Consider the mapping

$$z'=g(z)=z^2+c \ , \tag{2.1}$$

where $z=x+iy$ and c in general complex. The nature of the Julia set[15-18] can be understood by taking the case $c=0$. Then

$$\lim_{n\to\infty} g^n(z)=\begin{cases}\infty, & |z|>1\\ 0, & |z|<1 \ .\end{cases} \tag{2.2}$$

The borderline is the invariant circle $|z|=1$. For $C\neq 0$ the borderline is no longer smooth, but for c small enough it remains connected, and in fact is a Jordan curve (i.e., a curve that divides the plane into two parts—an inside and an outside).[21]

All the results reported below hold equally well for c real or complex. For the sake of exposition consider here the case of real c. In the range $-\frac{3}{4}<c<\frac{1}{4}$ the map has two real fixed points, where the smaller one is stable (and does not belong to the Julia set) and the large one is

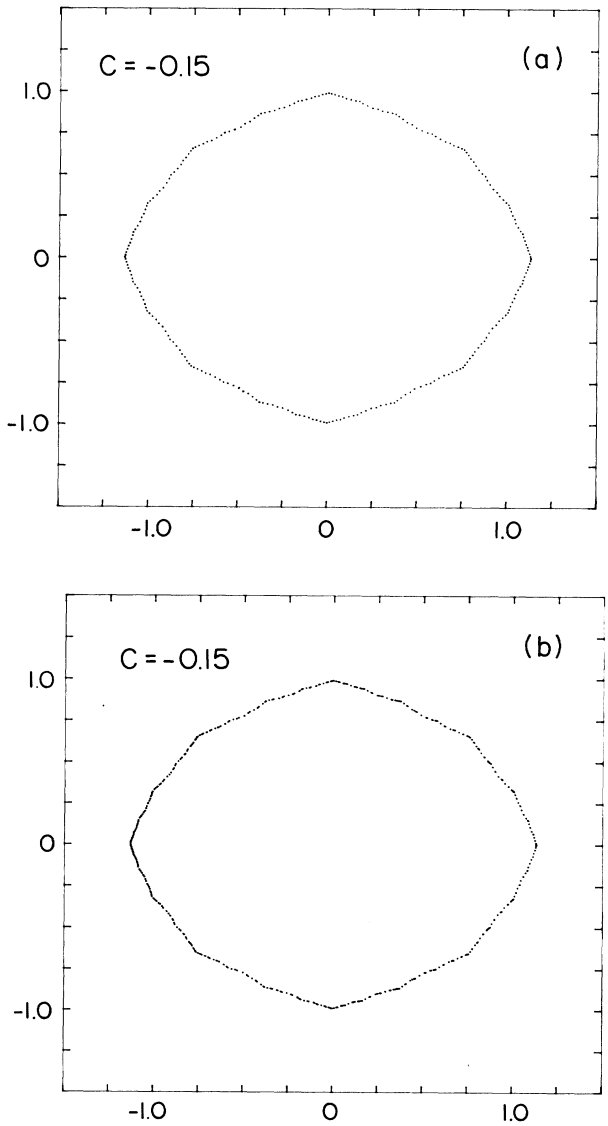

FIG. 1. The Julia set with $c=-0.15$. (a) All preimages up to order 8, (b) all periodic points up to order 8. The axes in this and the following figures are Imz and Rez.

unstable (and belongs to the set). The larger fixed point lies at the point $\bar{z}=\frac{1}{2}+(\frac{1}{4}-c)^{1/2}$. Here and below the sign of the square root is chosen with the convention that all surds have a non-negative imaginary part. If the imaginary part vanishes, the real part must be positive. This convention will be used below to define the symbol sequence. For small enough c including the range considered here, the Julia set is a Jordan curve. To get a graphic representation of this invariant set we cannot iterate the map forward, because the set is a repeller. We shall focus on two ways of generating the set. One is obtained from the preimages of the unstable fixed point, $\bar{z}=\frac{1}{2}+(\frac{1}{4}-c)^{1/2}$. Since the map is 2 onto 1, each point has two preimages. Thus at every level of the construction there are 2^n points, and we denote the set obtained at the nth step as $\mathcal{P}_n$. The other method of construction is achieved by considering all the periodic points of period n, i.e., $z=g^n(z)$. This set has 2^n-1 points, and is called below $\mathcal{J}_n$. As $n\to\infty$, the spatial distributions of the elements of these different sets approach one another. The Julia set is essentially this infinite-n limit. More technically, it is the closure of the union (over n) of either $\mathcal{J}_n$ or $\mathcal{P}_n$. In Fig. 1 we show the set with $c=-0.15$, where 1(a) was obtained from the preimages up to order 8, whereas 1(b) shows all the periodic points of order 8. We point out that although asymptotically the sets are the same, the first method picks the points that live on the most sharp "corners" of the figure, whereas the second method precisely avoids these points as much as possible. In Fig. 2 we show the set for $c=0.15$, and the same feature appears.

We must stress already here that the examples shown, i.e., $c=-0.15$ and $c=0.15$, are carefully chosen not to be too close to the boundary values $c=0.25$ and $c=-0.75$. In the vicinity of these points our scaling functions *do not converge well.* We believe that we understand the reasons for this, but the phenomena involved call for a separate study that is not undertaken here.

B. Symbolic representation

To proceed, we want to find a representation for every point on the Julia set. For the case in which the set is a closed curve this representation is particularly simple. All points in the set may be represented by the complex function U of the real variable t as

$$z=U(t)\ , \tag{2.3a}$$

where U is continuous. A consequence of the closed nature of the Jordan curve is that

$$U(t+1)=U(t)\ , \tag{2.3b}$$

when $c=0$, there is a very simple form of $U(t)$, namely, $U(t)=\exp(2\pi it)$. This choice makes the action of g upon U have the form

$$g(U(t))=U(2t)\ . \tag{2.3c}$$

One can prove that [see Ref. 14 (Peitgen-Richter), p. 57, Eq. 4.5] for all values of c for which the Julia set is a Jordan curve, there exist a $U(t)$ with the properties (2.3b) and (2.3c).

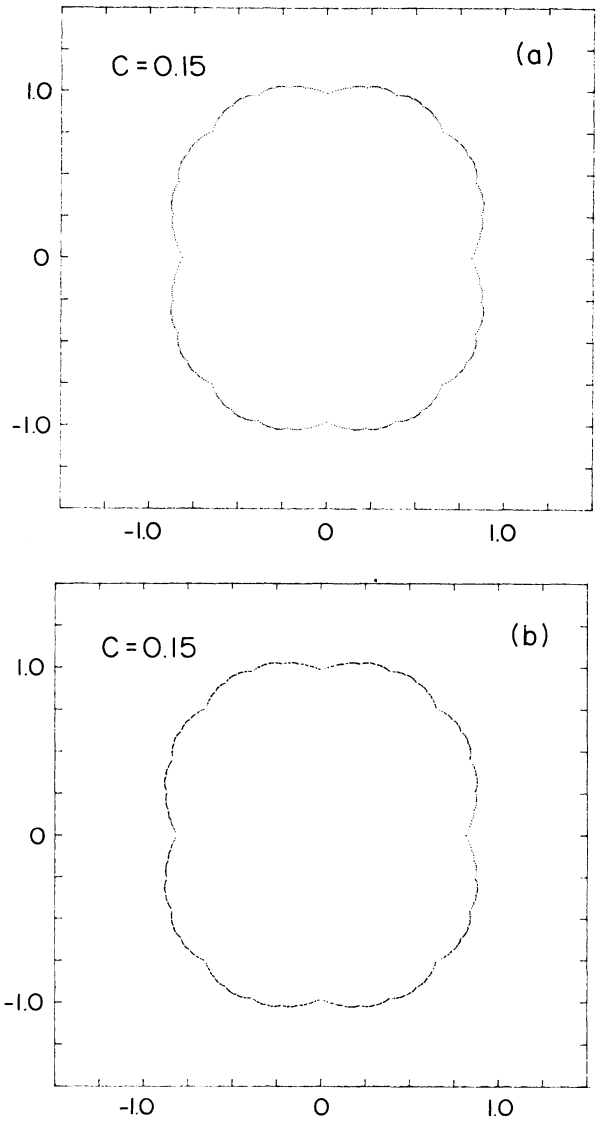

FIG. 2. The Julia set with $c=0.15$. (a) All preimages up to order 8. (b) All periodic points up to order 8.

To define the set $\mathcal{P}_n$ we wish to have all values of z such that $g^n(z)=\bar{z}$. These can be recursively constructed as

$$z(\varepsilon_1,\varepsilon_2,\ldots,\varepsilon_n)=\pm[z(\varepsilon_2,\varepsilon_2,\ldots,\varepsilon_n)-c]^{1/2}\ , \tag{2.4}$$

where $\varepsilon_1=0$ when the positive branch is used and $\varepsilon_1=1$ for a negative branch. Thus in $\mathcal{P}_n$, for example, $\bar{z}$ is denoted $z(0000)$, and its preimage is $z(1000)$. The set $\mathcal{P}_4$ is shown in Fig. 3(a) together with the symbol sequence of every point. It is evident that the position of a point mostly depends on ε_1 and only weakly on ε_n. We also notice that by interpreting $\varepsilon_1,\ldots,\varepsilon_n$ as the binary expansion of a number

$$t=\sum_{k=1}^{n}\varepsilon_k 2^{-k}\ , \tag{2.5}$$

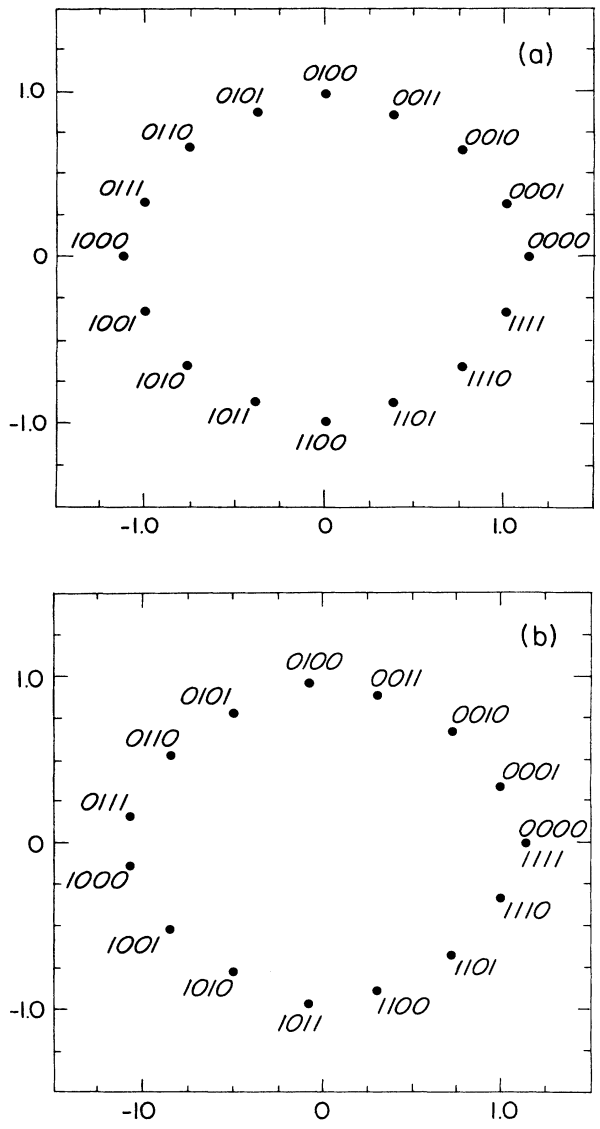

FIG. 3. (a) The points in $\mathcal{P}_4$ and the symbol sequence of every point. (b) The points in $\mathcal{J}_4$ and the symbol sequence of every point.

i.e., $z(\varepsilon_1,\ldots,\varepsilon_n)=U(t)$, the points of $\mathcal{P}_n$ are well ordered on the Jordan curve around the origin. Since the map is expansive the iteration has the effect of dropping one symbol from the sequence (i.e., it is a shift). Defining the operator S by

$$S(\varepsilon_1,\ldots,\varepsilon_n)=(\varepsilon_2,\ldots,\varepsilon_n)\ ,$$

$$S^{r-1}(\varepsilon_1,\ldots,\varepsilon_n)=(\varepsilon_r,\ldots,\varepsilon_n)\ ,$$

we see that for $r<n$

$$g^r z(\varepsilon_1,\ldots,\varepsilon_n)=z(\varepsilon_{r+1},\ldots,\varepsilon_n)$$
$$=z(S^r(\varepsilon_1,\ldots,\varepsilon_n))\ . \quad (2.6)$$

For brevity of notation we shall denote by Σ_1^n the sequence $(\varepsilon_1,\ldots,\varepsilon_n)$ and in general

$$\Sigma_r^m=(\varepsilon_r,\ldots,\varepsilon_m)\ . \quad (2.7)$$

Also we shall use

$$S(\Sigma_1^n)=(\varepsilon_2,\ldots,\varepsilon_n)\ ,\ \text{etc.} \quad (2.8)$$

For the set $\mathcal{J}_n$ the symbolic representation is also straightforward. We first realize that there are exactly 2^n-1 points in the set. A binary tree is again adequate. Dividing the plane by a horizontal line through the fixed point, we denote the upper half-plane by 0 and the lower half-plane by 1. The symbolic representation is obtained by defining the function $\mu(z)$:

$$\mu(z)=\begin{cases}0 & \text{if } z \text{ in upper half-plane}\\ 1 & \text{if } z \text{ in lower half-plane,}\end{cases}$$

and then assigning to each z in $\mathcal{J}_n$ the itinerary

$$\mu(z),\mu(g(z)),\ldots,\mu(g^{(n-1)}(z))\ .$$

The elements of $\mathcal{J}_n$ are again well ordered around the Jordan curve; see Fig. 3(b). The fixed point itself is either 0^∞ or 1^∞.

To distinguish the symbolic sequence of $\mathcal{J}_n$ from that of $\mathcal{P}_n$ we shall denote it as

$$\Xi_1^n=(\mu_1,\ldots,\mu_n) \quad (2.9)$$

and we associate to it the binary fraction

$$t=\sum_{k=1}^{n}\mu_k 2^{n-k}/(2^n-1)\ . \quad (2.10)$$

The dynamics in this case is a permutation. Defining the operator

$$P\Xi_1^n=\Xi_2^1=(\mu_2,\ldots,\mu_n,\mu_1)\ , \quad (2.11a)$$

$$P^r\Xi_1^n=\Xi_{r+1}^r=(\mu_{r+1},\ldots,\mu_n,\mu_1,\ldots,\mu_r)\ , \quad (2.11b)$$

we see that

$$g^r z(\Xi_1^n)=z(\Xi_{r+1}^r)\ . \quad (2.12)$$

As in the case of $\mathcal{P}_n$, the position of the points on the Jordan curve is mostly determined by the head $(\mu_1,\mu_2,\ldots)$ of the symbolic representation. The final property that we shall make use of in the sequel is that $U(t)$ is continuous so that as $n\to\infty$ the elements of $\mathcal{J}_n$ and $\mathcal{P}_n$ cover the entire Julia set.

III. SCALING FUNCTIONS: PHENOMENOLOGY

A. The Feigenbaum approach

In this subsection we describe the construction of a scaling function that depends mostly *on the tail* of the symbol sequence. The theoretical proof of this feature is deferred to Sec. IV. Here we simply show how the data are used and display the resulting scaling functions.

Consider the set $\mathcal{P}_n$. We define the distances $l^{(n)}(\Sigma_1^n)$ by

$$l^{(n)}(\Sigma_1^n)=\left|z\left(t+\frac{1}{2^n}\right)-z(t)\right|\ , \quad (3.1)$$

where t is the binary fraction (2.5). The distances defined in (3.1) are the nearest-neighbor distances in $\mathcal{P}_n$. Next we define the *local mothers* of these distances, denoted by $l^{(n-1)}(\Sigma_1^n)$, to be simply the nearest-neighbor distances of the previous generation

$$l^{(n-1)}(\Sigma_1^n)=l^{(n-1)}(\Sigma_1^{n-1}) \ . \tag{3.2}$$

In Fig. 4(a) we show $l^{(n)}$ and $l^{(n-1)}$ for $\mathcal{P}_4$. Next we define the daughter-to-mother ratio, or the scaling function, by

$$l^{(n)}(\Sigma_1^n)/l^{(n-1)}(\Sigma_1^n)=\sigma(\Sigma_1^n) \ . \tag{3.3}$$

Figures 5(a)–5(c) show $\sigma(\Sigma_1^n)$ as a function of the binary fraction (2.4) for $\mathcal{P}_3$–$\mathcal{P}_5$, $c=-0.15$; clearly the scaling functions are not nicely convergent. The reason is that this scaling function depends mostly on the tail of the symbolic sequence. To show this we reorder the numbers (3.3) by reading the binary number backwards according to

$$t'=\sum_{k=1}^{n}\varepsilon_k 2^k/2^{n+1} \ . \tag{3.4}$$

Figure 6 shows $\sigma(\Sigma_1^n)$ for $n=4,9$ as a function of the binary fraction t'. Evidently we get now a nice convergence. This convergence is displayed quantitatively in Table I. As a function of n of $\mathcal{P}_n$, we display the average difference between $\sigma(\Sigma_1^n)$ and $\sigma(\Sigma_1^{n-1})$ as well as the largest deviation. The exponential convergence is evident. The analogous scaling functions for $c=0.15$ are shown in Fig. 7.

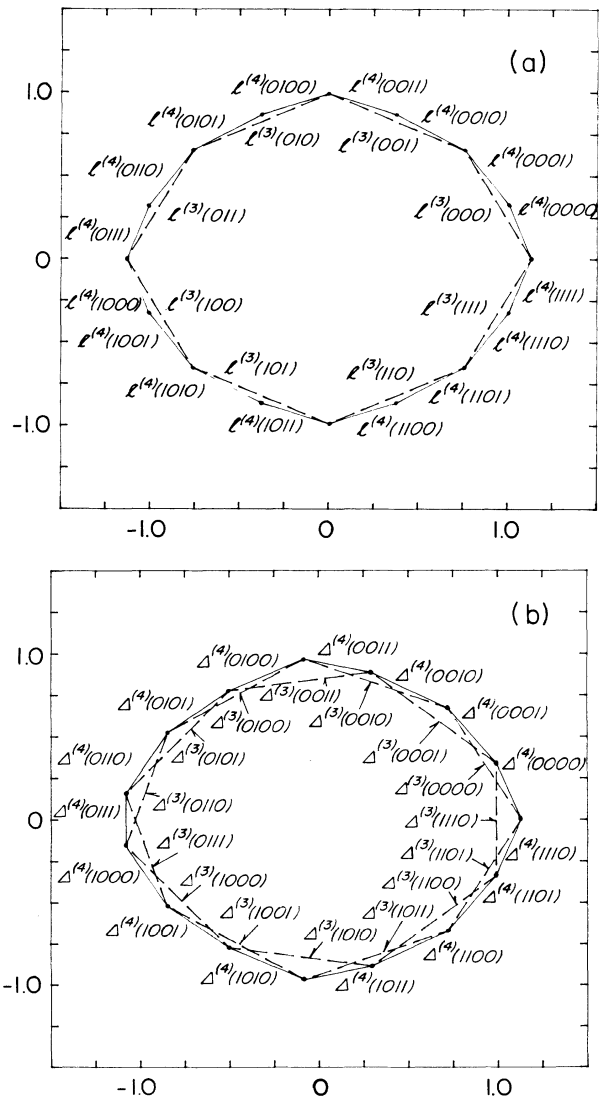

FIG. 4. (a) The distances $l^{(3)}$ and $l^{(4)}$ for $\mathcal{P}_4$. (b) The distances $\Delta^{(3)}$ and $\Delta^{(4)}$ for $\mathcal{T}_4$. The point 0000 can equally well be labeled 1111.

B. The RBS approach

In this section we construct scaling functions that depend mostly on *the head* of the symbol sequence. Again the theoretical proof is given in Sec. IV.

Consider the set $\mathcal{T}_n$. We define the smallest distances similarly to Eq. (3.1):

$$\Delta^{(n)}(\Xi_1^n)=|z(t+1/(2^n-1))-z(t)| \ , \tag{3.5}$$

where t is given by Eq. (2.10). The mothers, however, *are not local now.* Equation (3.2) is replaced by

$$\Delta^{(n-1)}(\Xi_2^1)=|z(2t+2/(2^n-1))-z(2t)| \ . \tag{3.6}$$

Notice that these mothers are precisely the map iterates of the daughters, and that we work within the $\mathcal{T}_n$ set. Figure 4(b) shows $\Delta^{(n)}$ and $\Delta^{(n-1)}$ for $\mathcal{T}_4$.

The scaling function $\tilde{\sigma}(\Xi_1^n)$ is defined now by

$$\tilde{\sigma}(\Xi_1^n)\equiv\frac{\Delta^{(n)}(\Xi_1^n)}{\Delta^{(n-1)}(\Xi_2^1)}=\frac{\Delta^{n}(\mu_1,\ldots,\mu_n)}{\Delta^{(n-1)}(\mu_2,\ldots,\mu_n,\mu_1)} \ . \tag{3.7}$$

It is easy to get figures that are as ugly as those in Fig. 5 if we plot (3.7) as a function of the number t' that worked so well for $\sigma(\Sigma_1^n)$. Here the dependence is strongest on $\mu_1,\mu_2,\ldots$ and we plot (3.7) as a function of t. As can be judged from Figs. 8 and 9, the convergence is rapid. Table II displays the convergence of these scaling functions in a similar way to Table I.

IV. SCALING FUNCTIONS: THEORY

In this section we analyze the scaling functions obtained via the two approaches presented in Sec. III, and derive their main property, i.e., the dependence on the head or tail of the symbol sequence. In addition, we relate the largest eigenvalue of the transfer matrix to the thermodynamics. In all that follows we shall assume that the derivative of the map is bounded from below, i.e., that there exists a number A such that

$$|dg(\Sigma_1^n)>A \tag{4.1}$$

for any Σ_1^n. This is equivalent to stating that $z=0$ does not belong to the set. We also shall make use of the (trivial) fact that d^2g is bounded from above (but $d^2g=2$).

Most straightforward is the analysis of σ of the $\mathcal{T}_n$ set. Since $\Delta^{(n-1)}$ is simply the map image of $\Delta^{(n)}$, we have for large n (i.e., Δ^n small)

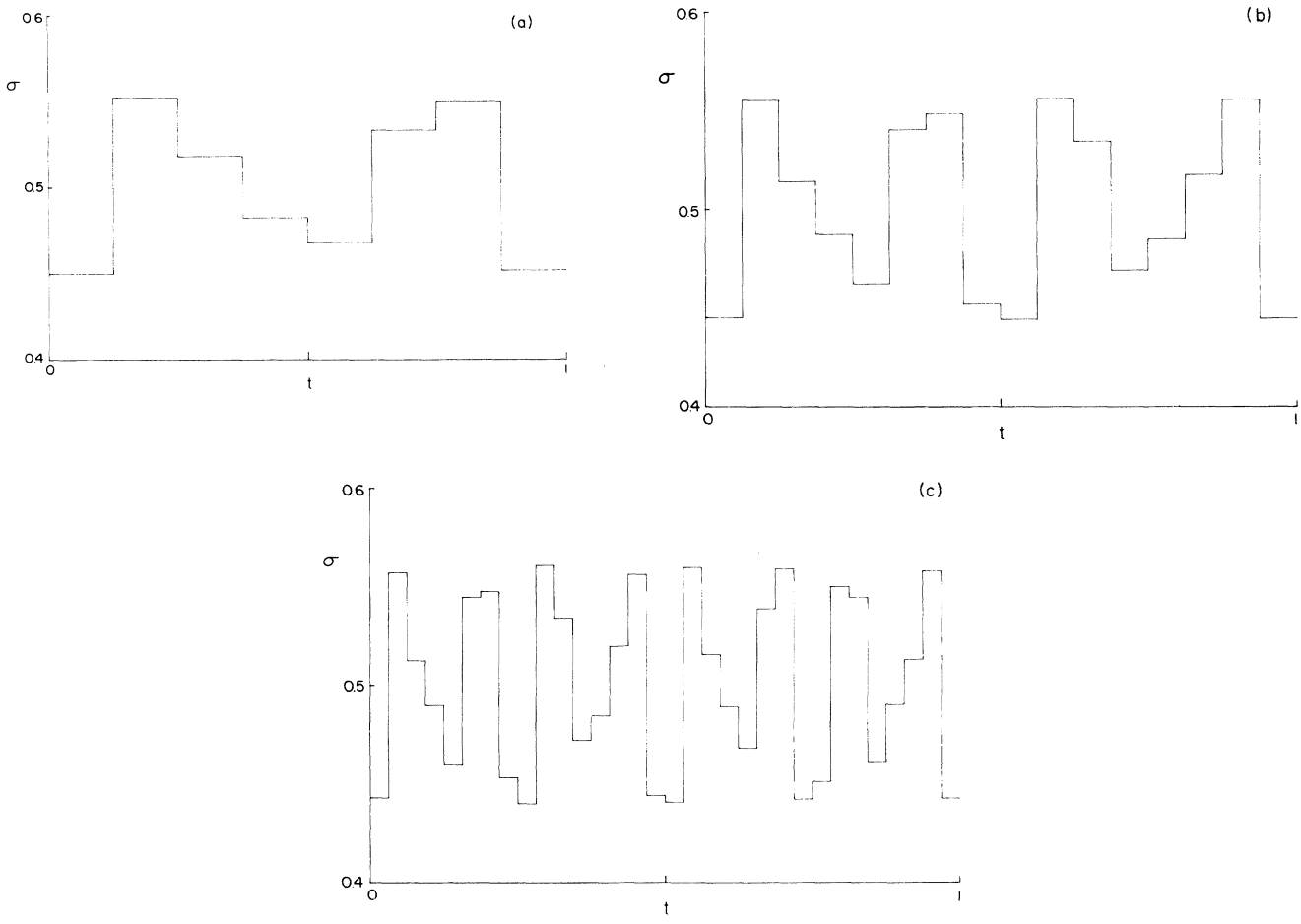

FIG. 5. The scaling function σ plotted vs t with $c=-0.15$. Note that the function does not converge. Parts (a), (b), and (c) represent, respectively, orders 3, 4, and 5.

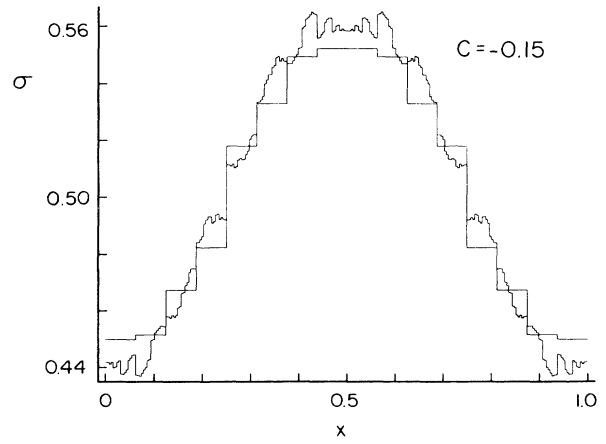

FIG. 6. Scaling functions with $c=-0.15$ for Feigenbaum approach. Shown are orders 4 and 9.

TABLE I. Convergence with Feigenbaum approach.

Order	Average error	Maximum error
	$c=-0.15$	
4	0.049 34	0.079 81
5	0.016 957	0.054 227
6	0.011 441	0.027 111
7	0.005 201 5	0.019 651
8	0.003 015 1	0.011 253
9	0.001 490 8	0.005 980 2
10	0.000 819 08	0.003 801 7
	$c=0.15$	
4	0.041 56	0.055 816
5	0.019 566	0.056 374
6	0.012 048	0.041 097
7	0.066 001 8	0.027 248
8	0.003 354 9	0.017 384
9	0.001 711 7	0.010 89
10	0.000 920 77	0.006 757 4

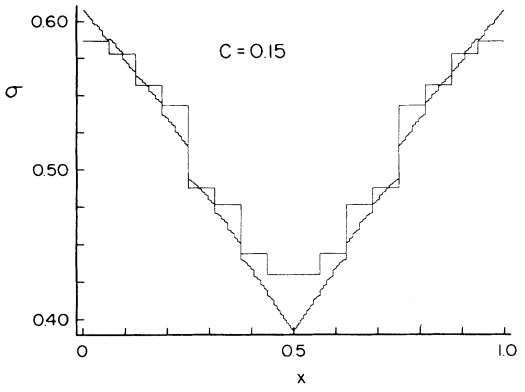

FIG. 7. Scaling functions with $c=0.15$ for RBS approach. Shown are orders 4 and 9.

TABLE II. Convergence with the RBS approach.

Order	Average error	Maximum error
	$c=-0.15$	
4	0.022 95	0.037 76
5	0.007 61	0.012 44
6	0.003 79	0.008 86
7	0.002 29	0.004 90
8	0.001 24	0.003 55
9	0.000 67	0.001 94
	$c=0.15$	
4	0.046 49	0.085 20
5	0.014 93	0.042 82
6	0.006 67	0.024 32
7	0.003 21	0.014 52
8	0.001 66	0.008 80
9	0.000 87	0.005 37

$$\Delta^{(n-1)}(P(\Xi_1^n))=|dg(\Xi_1^n)|\,\Delta^n(\Xi_1^n)\ , \tag{4.2}$$

where $dg(\Xi_1^n)$ is the derivative of the map at $z(\Xi_0^n)$. Equivalently,

$$\frac{\Delta^{(n)}(\mu_l,\ldots,\mu_n)}{\Delta^{(n-1)}(\mu_2,\ldots,\mu_n,\mu_1)}=\frac{1}{|dg(\Xi_1^n)|}\ . \tag{4.3}$$

Since the derivative is simply $2Z(\mu_1,\ldots,\mu_n)$, we see why the scaling function $\tilde{\sigma}(\mu_1,\ldots,\mu_n)$ depends most strongly on the head $(\mu_1,\mu_2,\ldots)$ of the symbol sequence.

Note now that Eq. (4.2) can be iterated to yield

$$\Delta^{(0)}=|dg(\Xi_l^n)dg(P(\Xi_l^n))\cdots dg(P^{n-1}(\Xi_l^n))|\,\Delta^{(n)}(\Xi_l^n)\ , \tag{4.4}$$

where $\Delta^{(0)}$ is of O(1). We thus have an estimate of $\Delta^{(n)}$ that can be used in Eq. (1.9) to yield

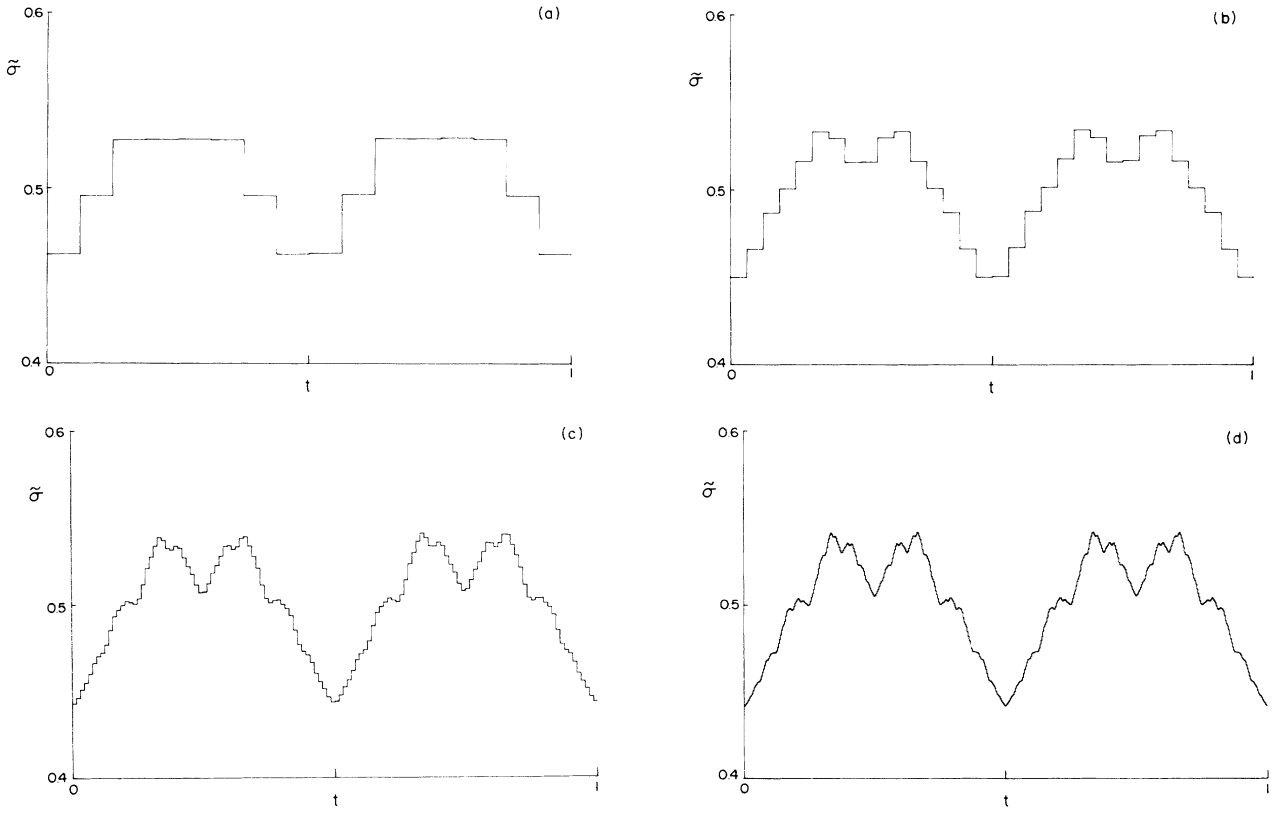

FIG. 8. Scaling functions with $c=-0.15$ for RBS approach. Shown are orders 4, 5, 7, and 9.

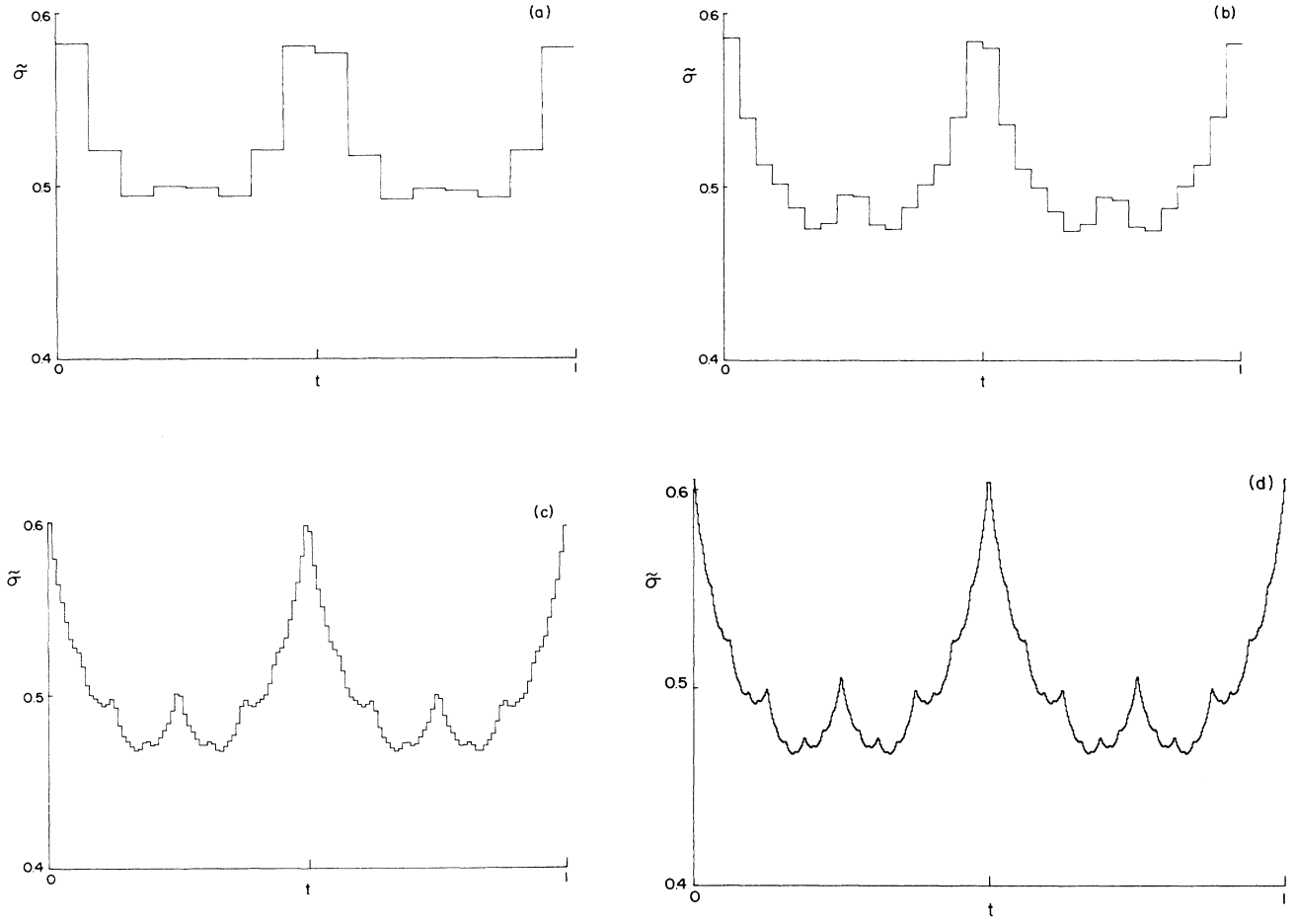

FIG. 9. Scaling functions with $c=0.15$ for RBS approach. Shown are orders 4, 5, 7, and 9.

$$(2^n-1)^{q(\tau)}=\sum_{\Xi_1^n\in\mathcal{I}_n}|dg(\Xi_1^n)|^{\tau}|dg(P(\Xi_1^n))|^{\tau}\cdots|dg(P^{n-1}(\Xi_1^n))|^{\tau}\ . \tag{4.5}$$

This equation can be written as a matrix product using the matrix M where

$$\langle\Xi\,|\,M(\tau)\,|\,\Xi'\rangle=\delta(\Xi',P(\Xi))\,|\,dg(\Xi)\,|^{\tau}\ . \tag{4.6}$$

Equation (4.5) becomes then

$$(2^n-1)^{q(\tau)}=\sum_{\Xi\in\mathcal{I}_n}\langle\Xi\,|\,M^n(\tau)\,|\,P^n(\Xi)\rangle \tag{4.7}$$

but since $P^n(\Xi)=\Xi$ we find

$$(2^n-1)^{q(\tau)}=\mathrm{tr}M^n(\tau)\ . \tag{4.8}$$

Since M depends only weakly on the tail of the symbolic sequence, Eq. (4.8) can be interpreted as a statement on a finite-size matrix, or

$$(2^n-1)^{q(\tau)}=\sum_{\alpha}M_{\alpha}^n(\tau)\ , \tag{4.9}$$

where M_α are the eigenvalues of M. In the limit $n\to\infty$ the largest eigenvalue $\lambda(\tau)$ is dominating and we recover Eq. (1.13)

$$2^{q(\tau)}=\lambda(\tau)\ . \tag{4.10}$$

Next we turn to the scaling function $\sigma(\Sigma_1^n)$ of the $\mathcal{P}_n$ set. As before, we estimate the lengths $l^{(n)}(\varepsilon_1,\ldots,\varepsilon_n)$ and $l^{(n-1)}(\varepsilon_1,\ldots,\varepsilon_n)$ using the derivative of the map

$$l^{(n)}(\Sigma_1^n)=|\,dg(z(\Sigma_1^n))\,|^{-1}l^{(n-1)}(\Sigma_2^{n-1}) \tag{4.11a}$$

and from Eq. (3.2)

$$l^{(n-1)}(\Sigma_1^n)l^{(n-1)}(\Sigma_1^{n-1})=|\,dg(z(\Sigma_1^{n-1}))\,|^{-1}l^{(n-2)}(\Sigma_2^{n-2})\ . \tag{4.11b}$$

We now find two estimates of

$$\sigma(\Sigma_1^n)=\frac{l^{(n)}(\Sigma_1^n)}{l^{(n-1)}(\Sigma_1^n)}\ .$$

By using both (4.11a) and (4.11b), we find

$$\sigma(\Sigma_1^n)\simeq\sigma(\Sigma_2^n)$$

since the dg factors are approximately equal. Hence $\sigma(\Sigma_1^n)$ depends only very weakly upon the leading digits of Σ_1^n. For this reason, we can write

$$\sigma(\Sigma_1^n)=\hat{\sigma}(\varepsilon_n,\varepsilon_{n-1},\varepsilon_{n-2},\ldots)\ . \tag{4.12}$$

But, from (4.11a) alone, we find

$$\sigma(\Sigma_1^n)=[l^{(n-1)}(\Sigma_1^{n-1})]^{-1}\,|\,dg(z(\Sigma_1^n))\,|^{-1}l^{(n-1)}(\Sigma_2^n)\ . \tag{4.13}$$

Repeating the steps (4.3)–(4.7) we find a transfer matrix K,

$$\langle\Sigma\,|\,K\,|\,\Sigma'\rangle=|\,\hat{\sigma}(\Sigma)\,|^{-\tau}\delta(\Sigma',\tilde{S}(\Sigma))\ , \tag{4.14}$$

where $\tilde{S}(\varepsilon_n,\ldots,\varepsilon_1)=(\varepsilon_{n-1},\ldots,\varepsilon_1)$. But in light of Eq. (4.13) we have

$$\langle\Sigma\,|\,K\,|\,\Sigma'\rangle=|\,l(\Sigma)\,|^{-\tau}\langle\Sigma\,|\,M\,|\,\Sigma'\rangle\,|\,l(\Sigma')\,|^{\tau}\ . \tag{4.15}$$

Thus K^n and M^n are similar, having the same eigenvalues. The thermodynamic information is equally extractable from either.

V. CALCULATING THERMODYNAMICS FROM LOW-ORDER DATA

Since the scaling functions converge rapidly, we ought to be able to estimate $q(\tau)$ or $f(\alpha)$ from low-order scaling functions. In this section we present results of such calculations and compare them to direct evaluations based on the highest-order $\mathcal{P}_n$ and $\mathcal{I}_n$ at our disposal. The direct data is taken from

$$2^{q(\tau)}=\frac{\sum_{\Sigma\in\mathcal{P}_{12}}|\,l^{(12)}(\Sigma)\,|^{-\tau}}{\sum_{\Sigma'\in\mathcal{P}_{11}}|\,l^{(11)}(\Sigma')\,|^{-\tau}} \tag{5.1}$$

and

$$\left[\frac{2^{10}-1}{2^9-1}\right]^{q(\tau)}=\frac{\sum_{\Xi\in\mathcal{I}_{10}}|\,\Delta^{(10)}(\Xi)\,|^{-\tau}}{\sum_{\Xi'\in\mathcal{I}_{10}}|\,\Delta^{(9)}(\Xi')\,|^{-\tau}}\ . \tag{5.2}$$

Not surprisingly, (5.1) and (5.2) give essentially the same $q(\tau)$ and the same $f(\alpha)$ curves. The $f(\alpha)$ curves are shown in Figs. 10 and 11.

Consider first the Feigenbaum approach. We have used for both $c=0.15$ and $c=-0.15$ the function $\sigma(\varepsilon_3,\varepsilon_2,\varepsilon_1)$ which contains in fact four independent scale factors, because σ has a twofold symmetry around $x=0.5$ (see Figs. 6 and 7). The matrix whose eigenvalue is calculated is

$$\langle\varepsilon_3,\varepsilon_2\,|\,T\,|\,\varepsilon_2',\varepsilon_1\rangle=\begin{array}{c}\\00\\01\\10\\11\end{array}\begin{array}{c}\begin{array}{cccc}00&01&10&11\end{array}\\\begin{pmatrix}\sigma_{\bar{0}\bar{0}\bar{0}}&\sigma_{\bar{0}\bar{0}\bar{1}}&0&0\\0&0&\sigma_{\bar{0}\bar{1}\bar{0}}&\sigma_{\bar{0}\bar{1}\bar{1}}\\\sigma_{\bar{0}\bar{1}\bar{1}}&\sigma_{\bar{0}\bar{1}\bar{0}}&0&0\\0&0&\sigma_{\bar{0}\bar{0}\bar{1}}&\sigma_{\bar{0}\bar{0}\bar{0}}\end{pmatrix}\end{array}\ . \tag{5.3}$$

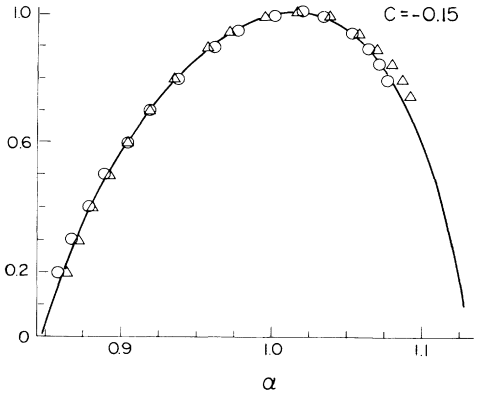

FIG. 10. $c=-0.15$. The solid curve is the $f(\alpha)$ spectrum obtained from direct calculations. The circles show results obtained from a four-scale approximation to the Feigenbaum scaling function. The triangles show results obtained from an eight-scale approximation to the RBS scaling function [shown in Fig. 8(b)].

The values of the scales, which we use, are basically obtained from averaging the limiting scaling function in each of eight equal intervals on the x axis. We obtain the numbers $\sigma_{000}=0.44$, $\sigma_{001}=0.48$, $\sigma_{010}=0.53$, $\sigma_{011}=0.565$ in the case $c=-0.15$ and the numbers $\sigma_{000}=-0.605$, $\sigma_{001}=0.545$, $\sigma_{010}=0.475$, $\sigma_{011}=0.4$ in the case $c-0.15$. We found $q(\tau)$ from Eq. (4.10) and, by employing Eqs. (1.5)–(1.7), calculated the $f(\alpha)$ function. The results are shown as the circles in Figs. 10 and 11. Clearly, this approach accomplishes prediction of the $f(\alpha)$ function to within 2–3 % over the whole q range for both c values.

The calculation via the RBS approach proceeds slightly differently. Starting from $\tilde{\sigma}(\varepsilon_0,\varepsilon_1,\varepsilon_2)$, we construct the matrix $M=\tilde{\sigma}(\Xi)\delta(\Xi,P(\Xi))$:

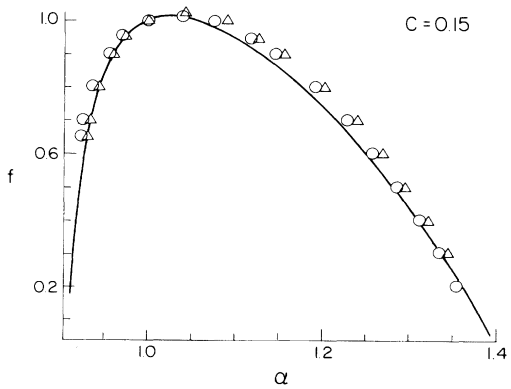

FIG. 11. $c=0.15$. The solid curve is the $f(\alpha)$ spectrum obtained from direct calculations. The circles show results obtained from a four-scale approximation to the Feigenbaum scaling function. The triangles show results obtained from an eight-scale approximation to the RBS scaling function [shown in Fig. 9(b)].

$$
\begin{array}{c|cccccccc}
 & 000 & 001 & 010 & 011 & 100 & 101 & 110 & 111 \\
\hline
000 & \tilde{\sigma}_{\overline{000}}^{\tau} & 0 & 0 & 0 & 0 & 0 & 0 & 0 \\
001 & 0 & 0 & \tilde{\sigma}_{\overline{001}}^{\tau} & 0 & 0 & 0 & 0 & 0 \\
010 & 0 & 0 & 0 & 0 & \tilde{\sigma}_{\overline{001}}^{\tau} & 0 & 0 & 0 \\
011 & 0 & 0 & 0 & 0 & 0 & 0 & \tilde{\sigma}_{\overline{000}}^{\tau} & 0 \\
100 & 0 & \tilde{\sigma}_{\overline{000}}^{\tau} & 0 & 0 & 0 & 0 & 0 & 0 \\
101 & 0 & 0 & 0 & \tilde{\sigma}_{\overline{001}}^{\tau} & 0 & 0 & 0 & 0 \\
110 & 0 & 0 & 0 & 0 & 0 & \tilde{\sigma}_{\overline{001}}^{\tau} & 0 & 0 \\
111 & 0 & 0 & 0 & 0 & 0 & 0 & 0 & \tilde{\sigma}_{\overline{000}}^{\tau}
\end{array}
\quad (5.4)
$$

Here we have used the fourfold symmetry of the RBS scaling functions (see Figs. 8 and 9) such that (5.4) only has two independent scales. For our calculations we however used $\tilde{\sigma}(\varepsilon_0,\varepsilon_1,\varepsilon_2,\varepsilon_3,\varepsilon_4)$ which are shown in Figs. 8(b) and 9(b). This function has eight independent scales and has already converged quite well. The resulting matrix has the size 32×32, but has a structure "similar" to (5.4). In the case $c=-0.15$ we use $\tilde{\sigma}_{00000}=0.451$, $\tilde{\sigma}_{00001}=0.466$, $\tilde{\sigma}_{00010}=0.4868$, $\tilde{\sigma}_{00011}=0.5005$, $\tilde{\sigma}_{00100}=0.5163$, $\sigma_{00101}=0.568$, $\tilde{\sigma}_{00110}=0.5293$, $\tilde{\sigma}_{00111}=0.5154$. In the case $c=0.15$ we use $\tilde{\sigma}_{00000}=0.6$, $\tilde{\sigma}_{00001}=0.502$, $\tilde{\sigma}_{00010}=0.513$, $\tilde{\sigma}_{00011}=0.52$, $\tilde{\sigma}_{00100}=0.488$, $\tilde{\sigma}_{00101}=0.455$, $\tilde{\sigma}_{00110}=0.479$, $\tilde{\sigma}_{00111}=0.495$. These values are taken directly from the scaling functions [Figs. 8(b) and 9(b)] except for the values of the extremas which are taken from the limiting scaling functions. Calculating now M^5 we use Eqs. (4.9) and (4.10) in the form ($n=5$):

$$31^{q(\tau)}=\lambda_{M^5}(\tau)\ ,$$

where λ_{M^5} is the largest eigenvalue of M^5. The results of the calculation for $f(\alpha)$ as shown as the triangles in Figs. 10 and 11 are comparable to the results of the Feigenbaum approach. In both approaches increasing the order of the matrices employed leads to a rapid convergence of the predicted thermodynamic functions.

VI. DISCUSSION

The main conclusion of this paper is that it is possible to develop a set of calculational tools that will help to determine the properties of multifractals; with a limited amount of information one can predict properties whose direct calculation calls for very detailed knowledge of the sets. The step performed here is a cautious one: We considered repellers—the simplest chaotic sets that exist off the borderline of chaos—and made heavy use of their "good" symbolic dynamics and their quasi-one-dimensionality.

For more general sets we expect that modifications of the formalism presented above would be needed. Firstly, we would lose the ability to work with scalar distances between data points. In general we shall need vector displacements $\Delta(\varepsilon_0,\ldots,\varepsilon_n)$. The scaling function will become then a matrix or, more generally, a tensor statement. Preliminary work in this direction indicates that this difficulty is surmountable and we hope to present results in the near future.

Another difficulty which is expected is the loss of adequate knowledge of the distribution of periodic orbits. Not only that we believe that the periodic orbits organize the motion, but for the general set we see no other obvious scheme for representing symbolically the members of the set. At any rate it appears that the difficulty of understanding the scaling structure of strange sets in dynamical systems is translatable to the concrete question of the distribution of periodic orbits.

As far as strange sets outside dynamical systems are concerned, we believe that the language developed above might find application there as well. The task of formulating specific applications remains, however, a future endeavor for the time being.

ACKNOWLEDGMENTS

This work has been supported in part by the Office of Naval Research. One of us (I. P.) acknowledges partial support by the Commission for Basic Research, administered by the Israel Academy of Sciences, and the Minerva Foundation.

*Present address: NORDITA, 2100 Copenhagen Ø, Denmark.
†Permanent address: Department of Chemical Physics, Weizmann Institute of Science, Rehovot 76100, Israel.

[1]B. B. Mandelbrot, J. Fluid Mech. **62**, 331 (1974).
[2]D. J. Farmer, Physica **4D**, 366 (1982).
[3]H. G. E. Hentschel and I. Procaccia, Physica **8D**, 435 (1983).
[4]P. Grassberger and I. Procaccia, Physica **13D**, 34 (1984).
[5]R. Benzi, G. Paladin, G. Parisi, and A. Vulpiani, J. Phys. A **17**, 352 (1984).
[6]U. Frisch and G. Parisi, in *Turbulence and Predictability in Geophysical Fluid Dynamics and Climate Dynamics*, edited by M. Ghil, R. Benzi, and G. Parisi (North-Holland, Amsterdam, 1985), p. 84.
[7]T. C. Halsey, M. H. Jensen, L. P. Kadanoff, I. Procaccia, and B. I. Shraiman, Phys. Rev. A **33**, 1141 (1986).
[8]T. C. Halsey, P. Meakin, and I. Procaccia, Phys. Rev. Lett. **56**, 854 (1986).
[9]D. Ruelle, Ergod. Th. Dynam. Sys. **2**, 99 (1982).
[10]R. Bowen, in *Equilibrium States and the Ergodic Theory of Anosov Diffeomorphisms*, Vol. 470 of *Lecture Notes in Math* (Springer, New York, 1975).
[11]Ya. Sinai, Russ. Math. Surv. **166**, 21 (1972).
[12]G. Julia, Commun. Pure Appl. Math. **4**, 47 (1918).
[13]B. B. Mandelbrot, Ann. N.Y. Acad. Sci. **357**, 249 (1980).
[14]R. L. Devaney, *An Introduction to Chaotic Dynamical Systems* (Benjamin/Cummins, Menlo Park, CA, 1986); H.-O. Peitgen and R. H. Richter, *The Beauty of Fractals* (Springer-Verlag, Berlin, 1986).

[15]J.-P. Eckmann and I. Procaccia, Phys. Rev. A **34**, 659 (1986).
[16]T. Bohr and D. Rand (unpublished).
[17]M. J. Feigenbaum, Los Alamos Sci. **1**, 4 (1980); Comm. Math. Phys. **77**, 65 (1980).
[18]M. J. Feigenbaum (unpublished).
[19]M. J. Feigenbaum, M. H. Jensen, and I. Procaccia, Phys. Rev. Lett. **57**, 1503 (1986).
[20]It is convenient to write (Ref. 3) $(q-1)D_q = \log \Sigma P_i^q / \log l$ and calculate the derivative.
[21]L. P. Kadanoff and C. Tang, Proc. Nat. Acad. Sci. U.S.A. **81**, 1276 (1984).
[22]C. Grebogi, E. Ott, and J. P. Yorke, Physica **7D**, 181 (1983).